nature climate change

ARTICLES

https://doi.org/10.1038/s41558-019-0602-x

The effect of plant physiological responses to rising CO_2 on global streamflow

Megan D. Fowler[1*], Gabriel J. Kooperman[2], James T. Randerson[1] and Michael S. Pritchard[1]

River flow statistics are expected to change as a result of increasing atmospheric CO_2 but uncertainty in Earth system model projections is high. While this is partly driven by changing precipitation, with well-known Earth system model uncertainties, here we show that the influence of plant stomatal conductance feedbacks can cause equally large changes in regional flood extremes and even act as the main control on future low latitude streamflow. Over most tropical land masses, modern climate predictions suggest that plant physiological effects will boost streamflow, overwhelming opposing effects of soil drying driven by the effects of CO_2 on atmospheric radiation, warming and rainfall redistribution. The relatively unknown uncertainties in representing eco-physiological processes must therefore be better constrained in land-surface models. To this end, we identify a distinct plant physiological fingerprint on annual peak, low and mean discharge throughout the tropics and identify river basins where physiological responses dominate radiative responses to rising CO_2 in modern climate projections.

The effects of climate change on the hydrologic cycle will probably alter river networks and floodplains globally. Improving our understanding of the drivers behind these changes is critical for increasing confidence in projections of future flow extremes. If the main driver of basin-wide hydrologic change is a result of atmospheric responses to CO_2 increases, then model development should focus on improving the representation of precipitation in Earth system models (ESMs), as this is frequently noted as a critical component of flood projection uncertainty[1–4]. The ability of plant physiological changes (stomatal closure at high CO_2) to modify extreme runoff has only recently received attention[5]. We posit that such ecosystem effects could be as important as precipitation for streamflow extremes, consistent with known first-order impacts on mean runoff and discharge[6–9], thus also requiring model improvement to reduce uncertainty.

The atmospheric (radiative) effects of rising CO_2 have been widely studied. Global mean precipitation is expected to increase, with the most extreme rates projected to intensify even more than the Clausius–Clapeyron rate[10–12]. Regionally, more frequent/intense precipitation can contribute to soil saturation, leading to higher streamflow or more frequent flooding. This is of particular concern in the tropics, where a multimodel ensemble suggests an increase in the frequency and intensity of heavy precipitation despite mean decreases[13].

However, atmospheric processes may not be the sole driver of streamflow changes in some regions. As the concentration of CO_2 rises, many plants respond by closing their stomata, which can lower the amount of water lost through transpiration[7,14,15]. While this effect may be offset at mid-latitudes by increased leaf area, the physiological response of stomata is an important mechanism regulating changes in evapotranspiration in densely forested tropical regions[16]. Decreases in transpiration and increases in water use efficiency can lead to higher antecedent soil moisture and, as a consequence, streamflow may increase even without a shift in precipitation statistics.

The relative roles of future radiative versus plant physiological responses in regulating flooding and seasonal streamflow changes have not been previously quantified. In part, this is due to the highly uncertain magnitude of the physiological response in observations, related to the difficulty of directly observing such changes over sufficiently long periods of time[17] and across a large range of sites[18]. Incorporating sparse observations into global-scale ESMs has led to wide variance in representation[19], with subsequent effects on river discharge being further hampered by the lack of sophisticated river routing models in most ESMs. The goals of this study were: (1) to assess the extent to which plant physiological effects modulate global flood frequency and seasonal streamflow relative to radiatively driven changes; and (2) to identify river basins where plant responses are dominant. In the case of the second goal, efforts to constrain the strength of the net physiological effects in nature (through carbon enrichment experiments[20,21] or regional simulations attempting to match observed streamflow changes) may prove most fruitful.

Physiological and radiative effects on extreme flooding

To separate the atmospheric and plant responses to elevated CO_2, we conduct a series of four fully coupled ESM experiments using the community Earth system model with biogeochemistry enabled (CESM1-BGC)[22,23]. The experiments are validated against flood and streamflow estimates from established Coupled Model Intercomparison Project Phase 5 (CMIP5) representative concentration pathway 8.5 (RCP8.5) multimodel means by Hirabayashi et al.[4] (hereafter H13) and Koirala et al.[24] (hereafter K14). Leaf area in the community land model (CLM4; ref. [25]) increases with enhanced CO_2 but no dynamic vegetation is represented (consistent with most CMIP5/6 models), which could limit a potential buffering effect from changes in forest area and associated evapotranspiration. The transpiration reduction in CLM4 may also be overestimated relative to observations[19,26,27], although the large spread among observational sites and comparison to other ESMs suggest that the model is not an extreme outlier[14].

In three sensitivity experiments, CO_2 was increased to quadruple its pre-industrial value (control experiment, CTRL; 285 ppm) at a rate of 1% yr^{-1}. This increasing concentration was applied to

[1]Department of Earth System Science, University of California Irvine, Irvine, CA, USA. [2]Department of Geography, University of Georgia Athens, Athens, GA, USA. *e-mail: mdfowler@uci.edu

the atmosphere and land in FULL (fully coupled experiment), only the atmosphere in RAD (radiative experiment) and only the land in PHYS (plant-physiological experiment), following the C4MIP experimental protocol[28,29] (where PHYS and RAD refer to the simulations' forcing rather than a specific mechanism in the complex regional responses). These experiments were extended for 50 yr at constant 1,140 ppm CO_2. We used daily runoff from the last 30 yr of each experiment (CTRL, FULL, PHYS and RAD) to hydrodynamically downscale river discharge using the catchment-based macroscale floodplain model (CaMa)[30]. This choice allows consistency with H13 but our main findings are insensitive to expanding to 50 yr (Supplementary Fig. 1). Although human management of rivers is not included in our analysis, we have confirmed that CaMa captures the geographic diversity of annual average streamflow (Methods and Supplementary Fig. 2) and that PHYS-induced ecosystem responses are consistent with previous studies (Supplementary Note and Supplementary Fig. 3).

To estimate flood frequency, we fit the 30-yr time series of annual maximum discharge at every location to an extreme value distribution (generalized extreme value, GEV) to compute the return period of a flood magnitude equivalent to the 100-yr flood in pre-industrial conditions (hereafter the $CTRL_{100}$ flood), following H13. We consider flood changes relative to this baseline return period of 100 yr; regions with increased (decreased) flooding thus have future return periods less (greater) than 100 yr. We limit our analysis to signals that are significant at 95% as measured across a large bootstrap ensemble (see Methods).

To confirm that our use of a single ESM produces flood shift patterns comparable to an established multimodel ensemble, we compared the resulting return period in FULL (Fig. 1a) with the CMIP5 analysis of H13 (Fig. 1b). Although the magnitude of return period varies between the two and varies based on how the extreme value distribution itself is defined (see Methods), the sign is reassuringly consistent—78.3% of locations in FULL show flood changes in the same direction as H13. In both cases, the $CTRL_{100}$ flood occurs at least twice as frequently over much of the tropics (blue shading in Fig. 1). Flood frequency decreases instead throughout western Europe, the northeast and east coasts of South America and parts of North America (red shading in Fig. 1a–d), where reduced mean precipitation (over eastern South America) or less spring snowmelt (high latitudes) tends to reduce runoff extremes.

Flood shifts in FULL are shown to be a result of both physiologically (Fig. 1c) and radiatively (Fig. 1d) driven changes in return period, while changes of similar magnitude are induced by either mechanism alone. Over the western Amazon, for example, increased flooding is primarily plant-driven, where dynamic mountain–forest interactions result in basin-wide precipitation rearrangement[16]. Increased flooding over much of South Asia is a result of radiatively forced changes, potentially due to intensification of the Indian summer monsoon rain[31]. A third class of region can be defined by concurrent changes in both PHYS and RAD, thus dividing the globe into three flood-driving regimes: PHYS-driven, RAD-driven and multiply stressed (Fig. 1e).

Eight regions with broadly consistent drivers are defined by rectangles in Fig. 1e and analysed further to determine the cause of increased flooding (Supplementary Note and Supplementary Tables 1–3). For multiply stressed regions (blue rectangles in Fig. 1e), PHYS leads to more frequent flooding through increased soil moisture, which we interpret as a direct effect of CO_2-induced transpiration decline (Supplementary Fig. 3) since it occurs despite increases in plant productivity, leaf area and surface shortwave radiation; all of those changes, with varying degrees of statistical significance, would tend to dry the soil (Supplementary Table 1 and Supplementary Fig. 3). When only the atmosphere responds to rising CO_2 (RAD), increased precipitation is probably the most important driver given the inability of other variables such as snowmelt,

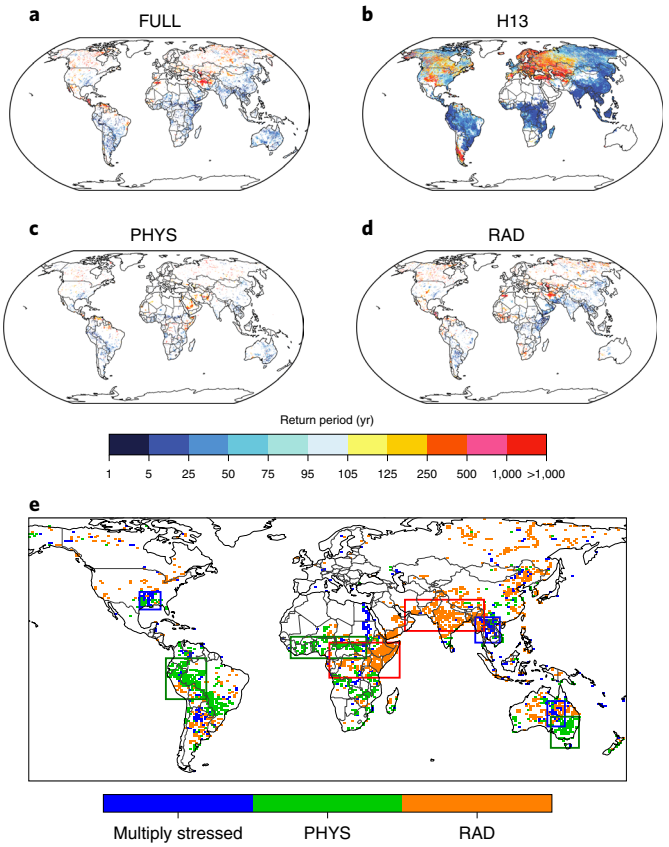

Fig. 1 | Frequency of the pre-industrial 100-yr flood under elevated CO_2 and its drivers. a,**b**, Return period of the historical 100-yr flood in FULL (**a**) versus the results of H13 for a multimodel average under RCP8.5 forcing (**b**). Dry regions masked as in Fig. 1 of H13[4]. **c**,**d**, PHYS (**c**) and RAD (**d**) as individual drivers (single forcings) of flood responses in FULL. **e**, Regional categorization of flood increases as primarily PHYS-driven (green), RAD-driven (orange) or a combination of both (blue) based on their contributions to the return period of the $CTRL_{100}$ flood in FULL. Results were omitted in **a** and **c**–**e** where insignificant at 95% confidence based on a large bootstrap ensemble (see Methods).

which is already near zero in these regions during the flood season, to explain the increased flooding. Other possible causative drivers, like increases in soil moisture and evapotranspiration, are difficult to disentangle from precipitation changes (Supplementary Table 1). Control by precipitation also dominates radiatively driven regions (orange rectangles in Fig. 1e and Supplementary Table 2), consistent with the expectation that warmer temperatures can promote higher mean precipitation and/or more frequent extremes, which can increase the likelihood of flooding.

Regions with plant-driven flood changes (green rectangles in Fig. 1e) experience more frequent flooding, not only as a result of increased soil moisture via direct stomatal closure but also through indirect precipitation effects, including mean precipitation increases over the western Amazon (Supplementary Note and Table 3)—in turn a result of complex interactions between surface energy partitioning, vertical vapour transport by planetary boundary layer turbulence and lateral vapour advection by regional orographic flow[16,32–34].

Plant physiological effects on annual streamflow metrics

Although CESM produces a striking physiological effect on floods, uncertainties in stomatal responses to CO_2 are large. Beyond a

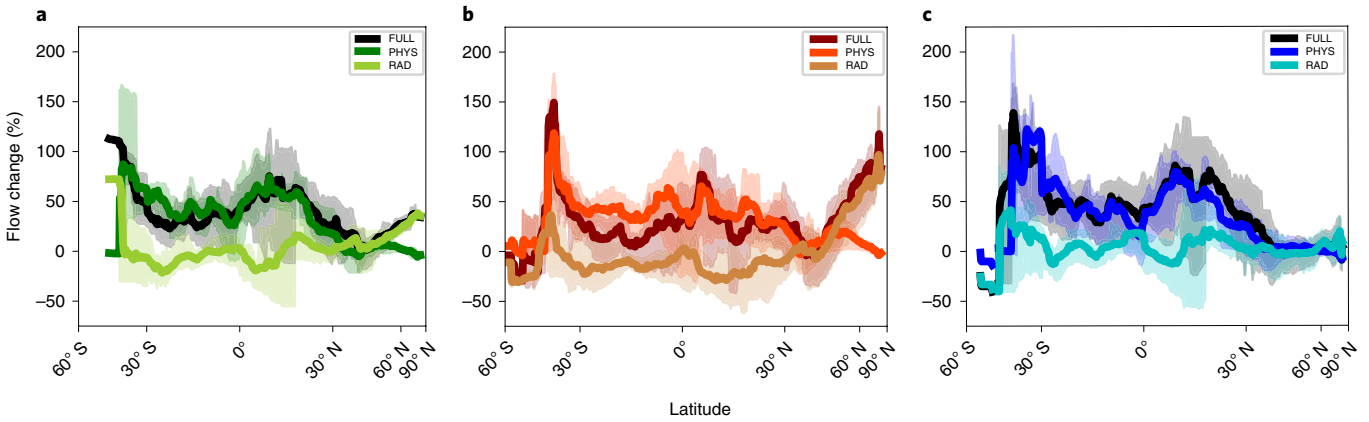

Fig. 2 | Changes in seasonal streamflow. a–c, Percentage change from CTRL in Q_{mean} (**a**), Q_{low} (**b**) and Q_{peak} (**c**). River gridcells with Q_{low} discharge <50 $m^3 s^{-1}$ or Q_{peak} <500 $m^3 s^{-1}$ in CTRL are not included (Supplementary Fig. 4). Latitudinal decompositions are smoothed with a 5° running mean; the shading denotes zonal variability as the interquartile range.

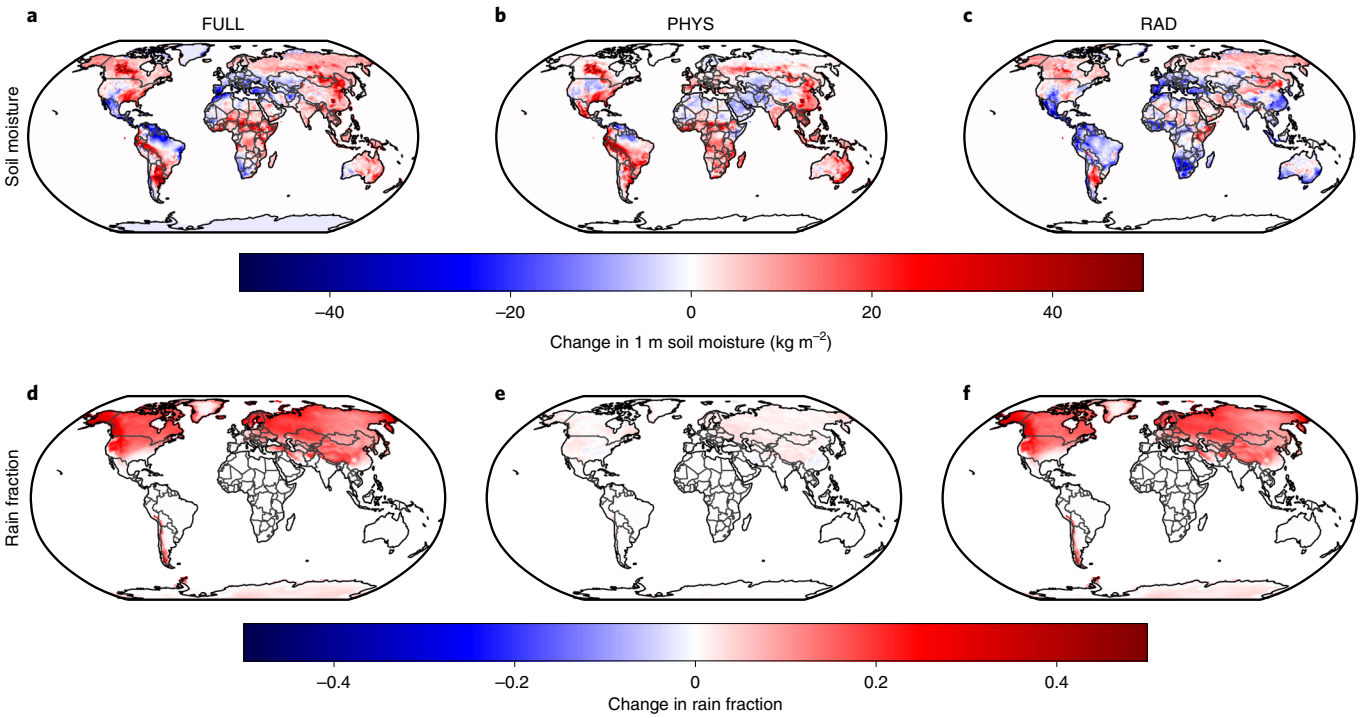

Fig. 3 | Changes in environmental conditions. a–f, Changes in 1 m soil moisture (top; **a–c**) and the fraction of precipitation that reaches the surface as rain instead of snow (bottom; **d–f**) relative to their values in CTRL for FULL (**a**,**d**), PHYS (**b**,**e**) and RAD (**c**,**f**). Mean differences are taken over the full 30-yr period.

handful of regional ecosystems that have been subjected to free-air CO_2 enrichment experiments[17,35], data are sparse, notably in the tropics; extending direct measurements to span a sufficient range of climates to constrain the magnitude of the stomatal response in ESMs is untenable. This motivates the need for indirect observable proxies of the plant physiological effect on streamflow in nature, as originally suggested by Gedney et al.[8]. If the same processes that produce large changes in extreme floods also modulate annual streamflow statistics, these—being more readily observable—could provide a useful metric for constraining net ecosystem responses to rising CO_2.

We investigate the seasonal cycle of streamflow, identifying broad regions and specific river basins where the PHYS effect rivals RAD contributions to FULL. Following K14, we compute annual mean (Q_{mean}), peak (Q_{peak}) and low (Q_{low}) flows for each river grid cell based on daily discharge, where seasonal extrema are defined as the 5th and 95th percentile flow rates annually, averaged to climatology.

We confirm the validity of CESM by comparing our results with CMIP5 mean changes from Fig. 1 of K14, as discussed in the Supplementary Note and Supplementary Fig. 5. In brief, FULL agrees well with the pattern of that multimodel average—79.2%, 80.5% and 68.0% of river grid cells in our experiment agree on the sign of Q_{mean}, Q_{peak} and Q_{low} changes respectively. The datasets generally agree in terms of large-scale spatial trends, showing increased Q_{peak} over much of the globe and concentrating the largest Q_{low} increases over northern latitudes (Supplementary Fig. 4).

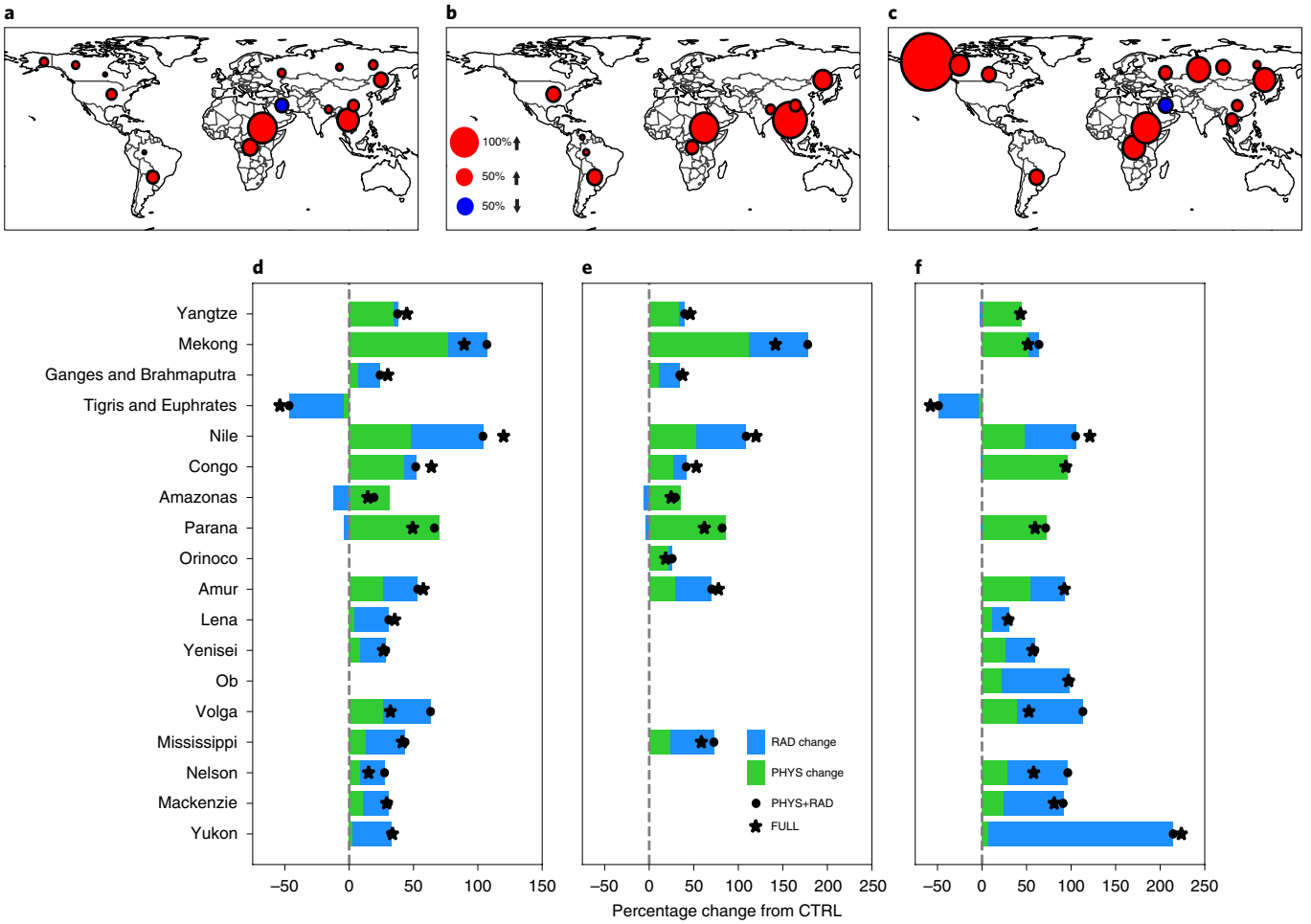

Fig. 4 | Basin-level streamflow percentage changes. a–c, FULL percentage changes in Q_{mean} (**a**), Q_{peak} (**b**) and Q_{low} (**c**) relative to CTRL. **d–f**, The contributions of ΔPHYS and ΔRAD to ΔFULL flow percentage changes. Black stars denote the FULL percentage change from CTRL (as shown by shaded circles in **a–c**). Black circles are the sum of ΔPHYS and ΔRAD. Coloured bars show the ΔPHYS (green) and ΔRAD (blue) percentage changes that support the total.

The key result here, however, is that plant physiological changes are the main control of these streamflow statistics (mean, seasonal peak and especially seasonal low flow) equatorward of 35°. PHYS plays a major role in driving dramatic Q_{low} increases throughout low latitude regions (Fig. 2a), which is linked primarily to higher soil moisture as a result of reduced stomatal conductance (Fig. 3b); rainwater simply becomes more prone to running off as increased plant water efficiency maintains a higher subsurface moisture reservoir that limits infiltration. Radiatively driven changes in Q_{low} tend to oppose this increase throughout the tropics due to increases in evaporative demand (Supplementary Fig. 6) but this is vastly overwhelmed by physiological effects in the zonal mean. Systematic increases in Q_{peak} and Q_{mean} equatorward of 45° N are again mostly controlled by plant responses, although radiatively driven changes in both cases are nearly neutral in the zonal mean (Fig. 2b). In the tropics and parts of the subtropics then, PHYS is almost solely responsible for increasing annual streamflow cycles across large portions of land.

At higher latitudes, the importance of atmospherically driven changes in RAD increases relative to plant-driven effects. Increases in all three streamflow metrics over much of high-latitude western Europe and North America can be linked to strong polar-amplified warming in RAD, which tends to reduce peak snowmelt rates (contributing to earlier and lower peak discharge in spring) and shift the ratio of falling precipitation towards rainfall at the expense of snow (Supplementary Fig. 6 and Fig. 3f). This change raises winter low flow by increasing runoff rather than allowing water to be stored in seasonal snowpack. The geographic disparity between tropical and higher latitude regions is summarized by pattern correlations in Supplementary Table 4.

Interestingly, PHYS also plays a non-negligible role in increasing Q_{low} and Q_{mean} across high-latitude continental interiors (Supplementary Fig. 4), with a signal that is strongest towards the southern edge of the boreal forest, that is decreasing with latitude, opposite to the polar-amplified warming effect of RAD and associated snow–rain transitions (Fig. 3). This might suggest the potential for an identifiable fingerprint of the physiological effect in unmanaged high-latitude river basins, with the caveat that radiative controls tend to dominate the FULL response poleward of 45° N. In the transition zone between PHYS- and RAD-dominated Q_{low} regimes, the influence of rising CO_2 on ecosystem processes allows for increasing vegetation cover in PHYS, yet transpiration reductions overwhelm these changes causing soil moisture to increase with a sharp boundary at the southern edge of the boreal forest region (Fig. 3).

Radiative and physiological effects on basin discharge

Our analysis allows us to separate the relative contributions of PHYS and RAD to changes in discharge for large river basins. We limit our attention to 18 of the 32 basins assessed (Supplementary

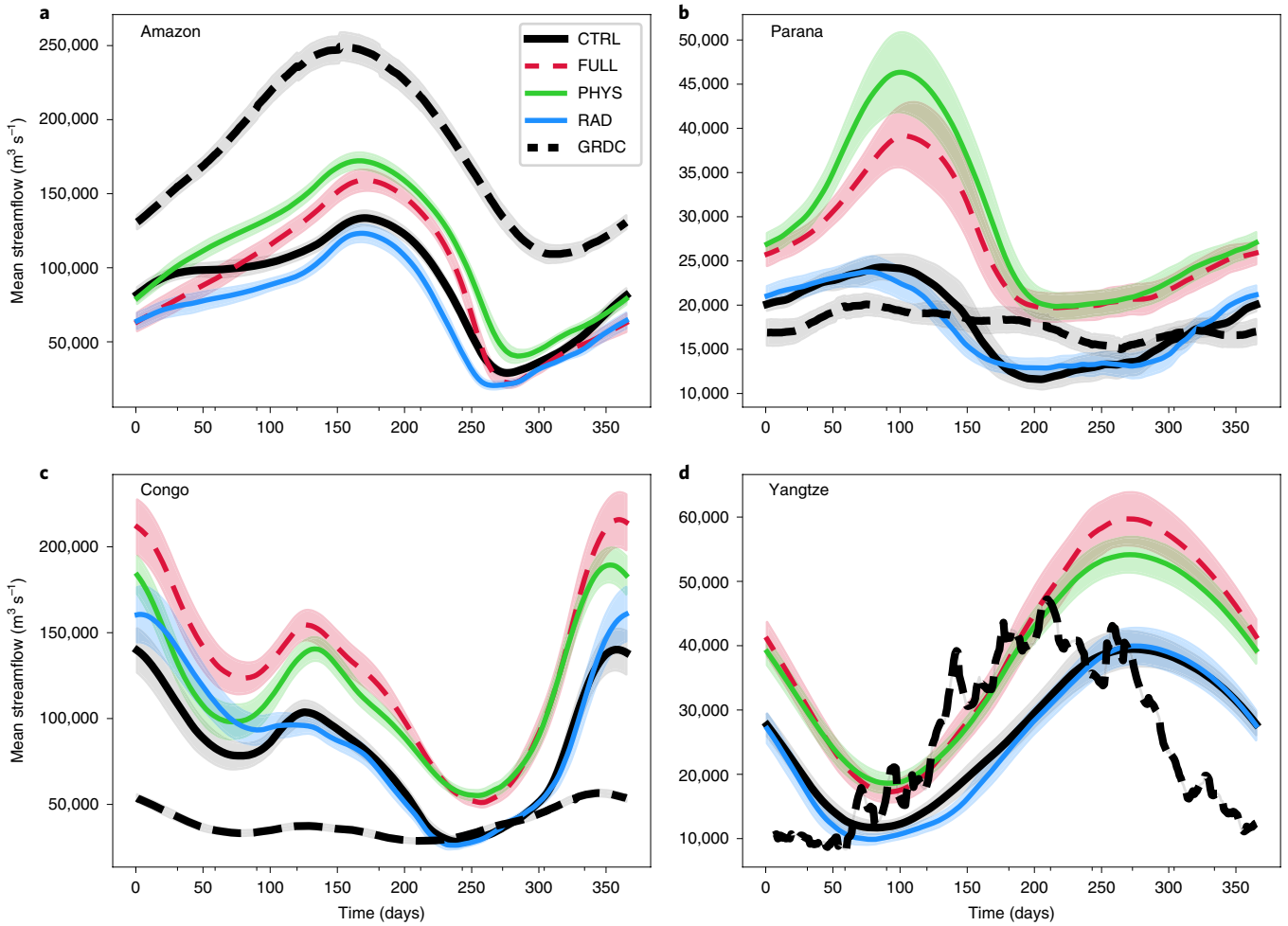

Fig. 5 | Average annual streamflow cycles at river outlets in PHYS-dominated basins. a, Amazon. **b**, Parana. **c**, Congo. **d**, Yangtze. Area-weighted average streamflow annual cycles near the outlets of each river. Dashed black lines represent nearby GRDC station data (all available years in the period 1970–2005) while coloured lines show modelled streamflow, where all grid cells within a quarter degree of the GRDC station have been averaged together. Error bars correspond to twice the standard error of discharge over the 30-yr period.

Fig. 7) in which the relative effects of PHYS and RAD on FULL are additive for mean, peak or low flow. In these basins, the residual of the following decomposition is small relative to the sum of PHYS and RAD, suggesting that the response of FULL can be explained by a linear combination of individual drivers,

$$\frac{\Delta\mathrm{FULL}}{\mathrm{CTRL}} = \frac{\Delta\mathrm{PHYS}}{\mathrm{CTRL}} + \frac{\Delta\mathrm{RAD}}{\mathrm{CTRL}} + \varepsilon \quad (1)$$

where ΔFULL, ΔPHYS and ΔRAD are the basin-averaged differences in streamflow from CTRL and ε is the residual, computed as the root mean square error between ΔFULL and the sum of ΔPHYS and ΔRAD across the 30-yr ensemble (Supplementary Fig. 8 and Supplementary Tables 5–7). The results of the decomposition are included in Fig. 4.

The primary driver of streamflow change can be identified by the dominant colour of the basin's bar in the bottom row of Fig. 4, with the magnitude of FULL indicated by the overall size of the circles in the top row. Again, basin responses are driven by PHYS, RAD or a combination of both: Mekong Q_{mean} and Q_{low} increases are primarily plant-driven, while the Yukon is almost exclusively radiatively driven. In general, the zonal pattern indicated in Fig. 2 is seen in Fig. 4 at the basin level as well, where tropical regions tend to be more strongly controlled by PHYS while high latitudes are more heavily affected by RAD.

Four basins stand out in particular as nearly exclusively plant-driven—the Amazon, Parana, Congo and Yangtze. Annual streamflow cycles in those basins reveal a systematic effect of PHYS to raise streamflow, which controls changes in FULL despite opposing changes in RAD (Fig. 5).

Details on these streamflow cycles and their comparison to observations are included in the Supplementary Note. In brief, despite a series of varying bias patterns in each basin—expected given ESM precipitation biases (Supplementary Fig. 10) and the exclusion of human water management in CaMa—the effect of reduced stomatal conductance is a systematic increase in streamflow across all months that is common to all four basins. This consistency adds confidence that the streamflow response to PHYS is a robustly simulated signal, in line with the observational findings of Gedney et al.[8] despite the fact that they did not allow for leaf area changes[36].

Discussion

Improved understanding of the physical mechanisms behind streamflow and flood frequency changes is critical for future ecosystem planning and management. Here, we have linked ESM experiments that isolate the plant physiological effects from

radiative effects of CO_2 on runoff to a hydrodynamic model that predicts their consequences for streamflow globally. Flood frequency analysis shows that plant physiological effects on the terrestrial water cycle are a first-order control on future shifts of the 100-yr flood.

Despite the major role of plants in the evolution of hydrological extremes under CO_2 forcing in CESM demonstrated here, the coupling between water and carbon cycles in modern land-surface models remains poorly constrained. To help address this source of uncertainty and complement sparse observational constraints, we use the model to identify fingerprints of plant physiological effects in observable metrics of annual streamflow. For low flows, the results show a competition in which the radiative effect tends to reduce but the physiological effect tends to increase seasonal flow minimums throughout low latitudes. At high latitudes, the relatively smaller net plant effect on mean and low flow expresses itself with an opposing meridional gradient to the polar-amplifying radiative effect across boreal forest watersheds. For peak flows, the plant response is the main driver of future changes throughout most low latitudes. Given this, we encourage more investigation of such fingerprints across multiple independent hydrodynamically downscaled ESMs, towards the hope of using observed streamflow to constrain the magnitude of buffered ecosystem responses to CO_2 in nature. The effect of the plant physiological response on hydrologic extremes across timescales is often overlooked in future climate projections but this work highlights the need to assess these effects more explicitly moving forward.

Online content

Any methods, additional references, Nature Research reporting summaries, source data, statements of code and data availability and associated accession codes are available at https://doi.org/10.1038/s41558-019-0602-x.

Received: 8 February 2019; Accepted: 11 September 2019;
Published online: 21 October 2019

References

1. Dankers, R. & Feyen, L. Climate change impact on flood hazard in Europe: an assessment based on high-resolution climate simulations. *J. Geophys. Res.* **113**, D19105 (2008).
2. Eisner, S. et al. An ensemble analysis of climate change impacts on streamflow seasonality across 11 large river basins. *Climatic Change* **141**, 401–417 (2017).
3. Shkolnik, I., Pavlova, T., Efimov, S. & Zhuravlev, S. Future changes in peak river flows across northern Eurasia as inferred from an ensemble of regional climate projections under the IPCC RCP8.5 scenario. *Clim. Dynam.* **50**, 215–230 (2018).
4. Hirabayashi, Y. et al. Global flood risk under climate change. *Nat. Clim. Change* **3**, 816–821 (2013).
5. Kooperman, G. J. et al. Plant-physiological responses to rising CO_2 modify simulated daily runoff intensity with implications for global-scale flood risk assessment. *Geophys. Res. Lett.* **45**, 1–10 (2018).
6. Betts, R. A. et al. Projected increase in continental runoff due to plant responses to increasing carbon dioxide. *Nature* **448**, 1037–1041 (2007).
7. Cao, L., Bala, G., Caldeira, K., Nemani, R. & Ban-Weiss, G. Importance of carbon dioxide physiological forcing to future climate change. *Proc. Natl Acad. Sci. USA* **107**, 9513–9518 (2010).
8. Gedney, N. et al. Detection of a direct carbon dioxide effect in continental river runoff records. *Nature* **439**, 835–838 (2006).
9. Lemordant, L., Gentine, P., Swann, A. S., Cook, B. I. & Scheff, J. Critical impact of vegetation physiology on the continental hydrologic cycle in response to increasing CO_2. *Proc. Natl Acad. Sci. USA* **115**, 4093–4098 (2018).
10. Allan, R. P. & Soden, B. J. Atmospheric warming and the amplification of precipitation extremes. *Science* **321**, 1481–1484 (2008).
11. Zhang, X., Wan, H., Zwiers, F. W., Hegerl, G. C. & Min, S.-K. Attributing intensification of precipitation extremes to human influence. *Geophys. Res. Lett.* **40**, 5252–5257 (2013).
12. Kooperman, G. J., Pritchard, M. S., Burt, M. A., Branson, M. D. & Randall, D. A. Impacts of cloud superparameterization on projected daily rainfall intensity climate changes in multiple versions of the Community Earth System Model. *J. Adv. Model. Earth Syst.* **8**, 1727–1750 (2016).
13. Chou, C., Chen, C., Tan, P. & Chen, K. T. Mechanisms for global warming impacts on precipitation frequency and intensity. *J. Clim.* **25**, 3291–3306 (2012).
14. Swann, A. L. S., Hoffman, F. M., Koven, C. D. & Randerson, J. T. Plant responses to increasing CO_2 reduce estimates of climate impacts on drought severity. *Proc. Natl Acad. Sci. USA* **113**, 10019–10024 (2016).
15. Leipprand, A. & Gerten, D. Global effects of doubled atmospheric CO_2 content on evapotranspiration, soil moisture and runoff under potential natural vegetation. *Hydrol. Sci. J.* **51**, 171–185 (2006).
16. Kooperman, G. J. et al. Forest response to rising CO_2 drives zonally asymmetric rainfall change over tropical land. *Nat. Clim. Change* **8**, 434–440 (2018).
17. Hovenden, M. & Newton, P. Plant responses to CO_2 are a question of time. *Science* **360**, 263–264 (2018).
18. Campbell, J. et al. Assessing a new clue to how much carbon plants take up. *Eos* https://doi.org/10.1029/2017EO075313 (2017).
19. De Kauwe, M. G. et al. Forest water use and water use efficiency at elevated CO_2: a model-data intercomparison at two contrasting temperate forest FACE sites. *Glob. Change Biol.* **19**, 1759–1779 (2013).
20. Ainsworth, E. A. & Long, S. P. What have we learned from 15 years of free-air CO_2 enrichment (FACE)? A meta-analytic review of the responses of photosynthesis, canopy properties and plant production to rising CO_2. *New Phytol.* **165**, 351–372 (2004).
21. Norby, R. J. et al. Model-data synthesis for the next generation of forest free-air CO_2 enrichment (FACE) experiments. *New Phytol.* **209**, 17–28 (2016).
22. Hurrell, J. W. et al. The Community Earth System Model: a framework for collaborative research. *Bull. Am. Meteorol. Soc.* **94**, 1339–1360 (2013).
23. Lindsay, K. et al. Preindustrial-control and twentieth-century carbon cycle experiments with the earth system model CESM1(BGC). *J. Clim.* **27**, 8981–9005 (2014).
24. Koirala, S., Hirabayashi, Y., Mahendran, R. & Kanae, S. Global assessment of agreement among streamflow projections using CMIP5 model outputs. *Environ. Res. Lett.* **9**, 1–11 (2014).
25. Lawrence, D. M. et al. Parameterization improvements and functional and structural advances in Version 4 of the Community Land Model. *J. Adv. Model. Earth Syst.* **3**, 1–27 (2011).
26. DeAngelis, A. M., Qu, X. & Hall, A. Importance of vegetation processes for model spread in the fast precipitation response to CO_2 forcing. *Geophys. Res. Lett.* **43**, 12550–12559 (2016).
27. Keller, K. M. et al. 20th century changes in carbon isotopes and water-use efficiency: tree-ring-based evaluation of the CLM4.5 and LPX-Bern models. *Biogeosciences* **14**, 2641–2673 (2017).
28. Friedlingstein, P. et al. Climate–carbon cycle feedback analysis: results from the C4MIP model intercomparison. *J. Clim.* **19**, 3337–3353 (2006).
29. Arora, V. K. et al. Carbon–concentration and carbon–climate feedbacks in CMIP5 earth system models. *J. Clim.* **26**, 5289–5314 (2013).
30. Yamazaki, D., Kanae, S., Kim, H. & Oki, T. A physically based description of floodplain inundation dynamics in a global river routing model. *Water Resour. Res.* **47**, 1–21 (2011).
31. Christensen, J. H. et al. in *Climate Change 2013: The Physical Science Basis* (eds Stocker, T. F. et al.) Ch. 14 (IPCC, Cambridge Univ. Press, 2013).
32. Richardson, T. B. et al. Carbon dioxide physiological forcing dominates projected Eastern Amazonian drying. *Geophys. Res. Lett.* **45**, 2815–2825 (2018).
33. Skinner, C. B., Poulsen, C. J., Chadwick, R., Diffenbaugh, N. S. & Fiorella, R. P. The role of plant CO_2 physiological forcing in shaping future daily-scale precipitation. *J. Clim.* **30**, 2319–2340 (2017).
34. Langenbrunner, B., Pritchard, M. S., Kooperman, G. J. & Randerson, J. T. Why does Amazon precipitation decrease when tropical forests respond to increasing CO_2? *Earth's Future* **7**, 450–468 (2019).
35. Nowak, R. S. CO_2 fertilization: average is best. *Nat. Clim. Change* **7**, 101–102 (2017).
36. Gerten, D., Rost, S., von Bloh, W. & Lucht, W. Causes of change in 20th century global river discharge. *Geophys. Res. Lett.* **35**, L20405 (2008).

Acknowledgements

M.D.F. and M.S.P. acknowledge primary support from the US Department of Energy Early Career Program (grant no. DE-SC0012152) and additional support from the National Science Foundation (grant no. AGS-1734164). G.J.K. and J.T.R. acknowledge support from the Gordon and Betty Moore Foundation (grant no. GBMF3269) and the RUBISCO science focus area supported by the Regional & Global Climate Modeling Program in the Climate and Environmental Sciences Division of the US Department of Energy, Office of Science. G.J.K. also acknowledges support from the US Department of Energy, Regional and Global Model Analysis Program (grant no. DE-SC0019459). CESM simulations were run and archived at the National Center for Atmospheric Research, Computational and Information Systems Laboratory on Yellowstone (P36271028).

Analysis was run in part on XSEDE supported systems Stampede2 (TG-ATM160016) and Comet (TG-ASC150024).

Author contributions

All authors contributed to the design of the experiment, interpretation of results and manuscript editing. G.J.K. performed the CESM simulations and M.D.F. performed the CaMa downscaling, carried out the analysis and drafted the initial manuscript with advice from M.S.P.

Competing interests

The authors declare no competing interests.

Additional information

Supplementary information is available for this paper at https://doi.org/10.1038/s41558-019-0602-x.

Correspondence and requests for materials should be addressed to M.D.F.

Peer review information *Nature Climate Change* thanks Robert Dickinson, Christopher Schwalm and the other, anonymous, reviewer(s) for their contribution to the peer review of this work.

Methods

CESM experiments. The four CESM1-BGC simulations include fully active atmosphere (CAM4)[37], land (CLM4)[25], ocean (POP2)[38] and sea ice (CICE4)[39] components, as described in Koopermen et al.[5]. CTRL was initialized from spun-up pre-industrial conditions with a fixed CO_2 concentration of 285 ppm that was maintained for 50 yr. Three additional experiments (FULL, RAD and PHYS) were then initialized from the end of CTRL to test the flood response to quadruple the amount of CO_2. In these simulations, the CO_2 concentration increased at 1% yr^{-1} over a 140-yr period and was then held fixed for an additional 50 yr. In RAD and PHYS, the land and atmosphere, respectively, experience the original 285 ppm of CO_2 rather than the increased value of 1,140 ppm when they are not the targeted response pathway, while in FULL both the land and atmosphere experienced the increased value. Global runoff from these 1° resolution simulations are interpolated to 0.5° via a bilinear cubic spline before being used in the CaMa model.

Hydrodynamic downscaling and extreme value curve fitting. For downscaling coarse resolution ESM output, we use the CaMa-Flood model (v.3.6.2), which uses daily runoff to generate high-resolution streamflow by solving a hydrodynamic flow equation[30]. This method of downscaling is well established in recent literature[3,4,24,40,41] and produces a reasonably accurate global river flow pattern[4,30]. Using runoff instead of precipitation as the driving boundary condition accounts for CO_2 impacts on both precipitation and evapotranspiration, while our experiment design allows us to separate the RAD and PHYS contributions to runoff changes. To ensure that CESM1-generated runoff is able to produce reasonable streamflow estimates when paired with CaMa, we compare CTRL river discharge with observations from 30 large river basins, as reported by the Global Runoff Data Centre (GRDC).
We take the same approach as in H13, choosing 30 river basins that meet spatial (areas larger than 150,000 km^2) and temporal requirements (at least 20 yr of data in the modern period of 1970–2000). Computing the correlation between the two datasets provides an estimate of how well the model can simulate streamflow (Supplementary Fig. 2). The reasonably good agreement provides some confidence that CESM is a useful tool for exploring future changes in streamflow originating from radiative and physiological effects of rising CO_2.

We consider two extreme value distributions to fit annual maximum discharge to, the Gumbel and the GEV. The pattern of flood frequency shifts created from this fitting is found to be insensitive to the choice of distribution, although the magnitude of the changes can vary significantly between the two (Supplementary Fig. 1). As a result, we focus here only on the regional distribution of changes and the relative contributions of PHYS and RAD to that pattern. These metrics are insensitive to the choice of curve fit.

We choose the GEV here on the basis of its simulation of less extreme frequency shifts and a reasonable value of the global average probability plot correlation coefficient (0.90). The GEV was then used to find the shape (ξ), location (μ) and scale (σ) parameters to estimate river discharge, $F(x)$:

$$F(x) = \exp\left(-\left(1+\xi\frac{(x-\mu)}{\sigma}\right)^{-\frac{1}{\xi}}\right) \quad (2)$$

The statistical fit to this distribution is carried out independently at each location and for each of the four experiments. The curve itself can thus be shifted based on the location parameter or stretched/shrunk based on the scale parameter, while additional characteristics like its skewness can be altered by changes in the shape parameter at every location. The magnitude of a given flood (U_T) can then be determined on the basis of return period (T) by inverting the cumulative distribution function of the GEV above:

$$U_T = \mu + \frac{\sigma}{\xi}\left(-\ln\left(1-\frac{1}{T}\right)^{-\xi}-1\right) \quad (3)$$

This is used to estimate the magnitude of the $CTRL_{100}$ flood. Equation (3) is then solved for T to determine the frequency of a flood with the $CTRL_{100}$ magnitude in each of the enhanced CO_2 experiments. Statistical confidence is built by limiting our analysis to signals that are significant at the 95% level, measured by a large bootstrap that is produced by randomly sampling with replacement the actual 30-yr annual maxima time series at each location and repeating the GEV fit 1,000 times.

Defining grid cells as RAD-driven, PHYS-driven or multiply stressed. To better isolate regions with flood increases that are driven by the atmospheric response (RAD-driven), the plant response (PHYS-driven) or by a combination of the two (multiply stressed), each grid cell is sorted on the basis of an agreement between the three experiments. RAD and PHYS flood frequency increases must both be at least 20% of the increase in FULL for a region to qualify as multiply stressed. Otherwise, the location is assigned to the driver with the larger change between the two. This practice is first carried out at the 0.25° CaMa-Flood resolution but is then scaled to the 1° CESM grid by identifying the mode of drivers within each larger CESM grid cell. Note that although the Nile region is particularly noticeable as a multiply stressed region (shown in blue in Fig. 1e), it is not selected for detailed analysis due to the high aridity of the region.

Data availability

The relevant datasets generated during this analysis are available at http://portal.nersc.gov/archive/home/m/mdfowler/www/. The full CESM output record is archived and available upon request. Data used to create Fig. 1b were received via personal correspondence with Y. Hirabayashi and requests should be directed to her (hyukiko@shibaura-it.ac.jp)[4]. Similarly, CMIP5 multimodel mean streamflow data used for comparison between FULL and K14 were received via personal communication with the lead author and should be requested from S. Koirala (skoirala@bgc-jena.mpg.de)[24]. Full CESM output is archived at the National Center for Atmospheric Research. Global Runoff Data Base observations in Fig. 5 are freely available from GRDC but cannot be redistributed by the author; requests should be sent directly to GRDC.

Code availability

All scripts that replicate the results of this study are accessible at https://github.com/megandevlan/Physiology-Streamflow. Data associated with these scripts are included in the repository, with a few exceptions. Relevant CESM and CaMa output are not included due to their size but are available at http://portal.nersc.gov/archive/home/m/mdfowler/www/. Data obtained from Y. Hirabayashi, S. Koirala and from the GRDC are not included and should be requested from the sources independently. The CaMa model itself can be obtained by emailing the developer, D. Yamazaki (yamadai@rainbow.iis.u-tokyo.ac.jp), while CESM is publicly available through a Subversion code repository—see http://www.cesm.ucar.edu/models/cesm1.0/ for more details.

References

37. Neale, R. B. et al. *Description of the NCAR Community Atmosphere Model (CAM 4.0)* Technical Note TN-486 (NCAR, 2010).
38. Smith, R. et al. *The Parallel Ocean Program (POP) Reference Manual* Technical Report LAUR-10-01853 (Los Alamos National Laboratory, 2010).
39. Hunke, E. C. & Lipscomb, W. H. *CICE: The Los Alamos Sea Ice Model Documentation and Software User's Manual Version 4.1* Technical Report LA-CC-06-012 (Los Alamos National Laboratory, 2010).
40. Hirabayashi, Y., Kanae, S., Emori, S., Oki, T. & Kimoto, M. Global projections of changing risks of floods and droughts in a changing climate. *Hydrol. Sci. J.* **53**, 754–772 (2008).
41. Pappenberger, F., Dutra, E., Wetterhall, F. & Cloke, H. L. Deriving global flood hazard maps of fluvial floods through a physical model cascade. *Hydrol. Earth Syst. Sci.* **16**, 4143–4156 (2012).